Phytomedicine 62 (2019) 152963

Contents lists available at ScienceDirect

Phytomedicine

journal homepage: www.elsevier.com/locate/phymed

Original Article

Byakangelicin as a modulator for improved distribution and bioactivity of natural compounds and synthetic drugs in the brain

Yoon Young Kang, Jihyeon Song, Jun Yeong Kim, Heesun Jung, Woon-Seok Yeo, Yoongho Lim, Hyejung Mok*

Department of Bioscience and Biotechnology, Konkuk University, 120 Neungdong-ro, Gwangjin-gu, Seoul 05029, Republic of Korea

ARTICLE INFO

Keywords:
Byakangelicin
Ex vivo monitoring
Compound mixture
Synergistic biodistribution
Brain

ABSTRACT

Background: The elucidation of the biological roles of individual active compounds in terms of their *in vivo* biodistribution and bioactivity could provide crucial information to understand how natural compounds work together as treatments for diseases.

Purpose: We examined the functional roles of Byakangelicin (Byn) to improve the brain accumulation of active compounds, *e.g.*, umbelliferone (Umb), curcumin (Cur), and doxorubicin (Dox), and consequently to enhance their biological activities.

Methods: Active compounds were administered intravenously to mice, with or without Byn, after which organs were isolated and visualized for their *ex vivo* fluorescence imaging to determine the bio-distribution of each active compound *in vivo*. For the *in vivo* bioactivity, Cur, either with or without Byn, was administered to a lipopolysaccharide (LPS)-induced neuro-inflammation model for 5 days, and its anti-inflammatory effects were examined by ELISA using a brain homogenate and serum.

Results: We successfully demonstrated that the levels of active compounds (Umb, Cur, and Dox) in the brain, lung, and pancreas were greatly elevated by the addition of Byn via direct *ex vivo* fluorescence monitoring. In addition, sufficient accumulation of the active compound, Cur, greatly reduced LPS-induced neuro-inflammation *in vivo*.

Conclusion: Byn could serve as a modulator to allow improved brain accumulation of diverse active compounds (Umb, Cur, and Dox) and enhanced therapeutic effects.

Introduction

Byakangelicin (Byn) is one of the active compounds found in the roots of *Angelica (A.) gigas*, commonly called “Danggui” in Korean, which originates from Korea (Sarker and Nahar, 2004). *A. gigas* has been widely used as a traditional medicine for the treatment of various neuronal diseases (Kim et al., 2016; Oh et al., 2015a; Sowndhararajan and Kim, 2017). In particular, extract of *A. gigas* has shown effective protection of neurons from cell death for ischemia mice and memory impaired mice (Oh et al., 2015b; Yan et al., 2004). However, the molecular mechanism of each compound in *A. gigas* for neural effects has not been well elucidated. In addition, compound mixtures from *A. gigas* are more pharmacologically active than any single active compound (Kan et al., 2008; Lee et al., 2009). Despite the strong and convincing biological activity of single compounds, including decursin (Dec), decursinol (Del), byakangelicol (Byl) *in vitro*, single compounds derived from natural extracts have usually shown poor efficacy *in vivo*, compared with compound mixtures (Fantini et al., 2015). In addition, although the mechanisms for many single compounds from natural extracts have been delineated, the mechanism behind the synergistic effects of compound mixtures or natural extracts has not been clearly elucidated.

Thus far, numerous studies examining the effects of drug combinations have focused on the investigation of the effects on drug metabolism, absorption, and activity *in vitro* after extraction (Rubio et al., 2013). Both resveratrol and mulberry, composed of quercetin and other polyphenols, can elicit changes in the metabolism and absorption of co-administered drugs by enhancing or inhibiting the activities of P-

Abbreviations: A., Angelica; Ang, Angelicin; Ang/Umb, Ang/Umb mixture; Byl/Umb, Byl/Umb mixture; Byn, Byakangelicin; Byn/Umb, Byn/Umb mixture; Byl, Byakangelicol; Cur, curcumin; Dec, Decursin; Dec/Umb, Dec/Umb mixture; Del, decursinol; Dox, doxorubicin; FBS, fetal bovine serum; FI, fluorescence intensity; LPS, lipopolysaccharide; PBS, phosphate-buffered saline; Umb, umbelliferone

* Corresponding author.
E-mail address: hjmok@konkuk.ac.kr (H. Mok).

https://doi.org/10.1016/j.phymed.2019.152963
Received 21 November 2018; Received in revised form 8 May 2019; Accepted 16 May 2019

glycoprotein (P-gp) and cytochrome P450s (CYPs) (Hsu et al., 2013). In combination of silybin and piperin, biliary excretion and metabolism of silybin were inhibited by piperin (Bi et al., 2019). Reversible and irreversible interactions of polyphenols with plasma proteins could also weaken the bioactivity of polyphenols such as their antioxidant activity (Xiao and Kai, 2012). However, changes in the bio-distribution of active compounds in the presence of other polyphenols have rarely been reported. In addition, most bio-distribution studies of active compounds were examined by HPLC and NMR analyses after extraction of samples from tissues/organs, because it is difficult to directly monitor single compounds. However, the direct monitoring of a compounds bio-distribution might be especially crucial for unstable natural compounds such as polyphenols. Recently, we have reported the pharmacokinetic changes of compounds, *e.g.* natural polyphenols and coumarins, through their interactions with other chemicals or drugs by direct *ex vivo* monitoring of fluorescent compounds (Kang et al., 2016b).

In this study, we examined the Byn, a representative component of *A. gigas*, as a modulator of the bio-distribution of active compounds in an *in vivo* model. It has been hypothesized that the excellent therapeutic effects of *A. gigas* in neuronal diseases might be attributed to a synergistic enhancement of the brain accumulation of active compounds by Byn. The accumulation of active compounds *e.g.* polyphenols and anticancer drugs, in the brain, lung, and pancreas could be easily and directly assessed via the *ex vivo* fluorescent imaging of selected fluorescent active compounds including umbelliferone (Umb, 7-hydroxycoumarin), curcumin (Cur), and the anticancer drug doxorubicin (Dox) after intravenous injection. The improved localization of active compounds in the presence of Byn was analyzed at diverse Byn/other compound weight ratios. As a control compound, other compounds from *A. gigas,* including Angelicin (Ang), Byl, nodakenin (Nod), and Dec were also examined by *ex vivo* fluorescent imaging of each tissue, tracking the fluorescence intensity (FI) of the active compounds. To explore if the enhanced localization of the active compounds in the brain could elicit improved biological activities, we examined the effects of Cur and Byn/Cur mixtures in an LPS-induced mouse neuro-inflammation model. The brain anti-inflammatory effects of the Byn/Cur mixture were quantitatively analyzed by measuring cytokine levels, including tumor necrosis factor α (TNF-α) and interleukin-1β (IL-β), in brain homogenates and serum by ELISA.

Materials and methods

Materials

Cur (purity ≥ 65% based on HPLC analysis), Umb (purity ≥ 98% based on HPLC analysis), Evan's blue (Eb), dimethyl sulfoxide (DMSO), ethyl acetate, ethanol, kolliphor, sodium dodecyl sulfate (SDS), 37% formaldehyde, and lipopolysaccharide (LPS) were purchased from Sigma-Aldrich (St. Louis, MO, USA). Byn, Dec, Del, Nod, and Ang were purchased from Chengdu Biopurify Phytochemicals Ltd. (Chengdu, Sichuan, China). They were used as provided by the manufacturer, whose purities were approximately 98% based on the HPLC analysis. Dox was purchased from Wako Pure Chemical Industries, Ltd. (Osaka, Japan). Terrell Isoflurane was purchased from Piramal Critical Care, Inc. (Bethlehem, PA, USA). The mouse TNF-α enzyme-linked immunosorbent assay (ELISA) kit was obtained from BD Biosciences (Franklin Lake, NJ, USA). The mouse IL-1β ELISA kit was obtained from R&D system (Minneapolis, MN, USA). The Micro-BCA protein assay kit was purchased from Pierce (Rockford, IL, USA). Vectashield Mounting Medium (with DAPI) was purchased from Vector Laboratories, Inc. (Burlingame, CA, USA). ICR mice (six-week-old, female) were purchased from DooYeol Biotech (Seoul, Korea). C57BL/6 mice (six-week-old, female) were purchased from Orient Bio Inc. (Seongnam, Gyunggi-do, Korea). All other chemicals were of analytical grade.

In vitro fluorescence imaging

Stocks of single compounds (Umb, Byn, Dec, and Ang) in DMSO were diluted with injection buffer (PBS containing 13.5% (v/v) kolliphor) at a final concentration of 50 μg/ml. Umb mixtures (Byn/Umb, Dec/Umb, and Ang/Umb) in DMSO were diluted with injection buffer at a constant Umb concentration of 50 μg/ml (weight ratio of other compound/Umb of 1). After the samples were loaded into 96-well black plates, the FIs were analyzed using Lago-X (Spectral Instruments Imaging, AZ, USA) at an excitation and emission wavelength of 360 and 490 nm, respectively.

Ex vivo fluorescence imaging of Umb

All animal care and experimental procedures were approved by the Animal Care Committee of Konkuk University. ICR mice were injected intravenously with Umb compounds in injection buffer at an Umb dose of 160 and 320 mg/kg, and incubated for 15 min. Each organ, including the brain, heart, lung, kidney, pancreas, liver, and spleen were isolated and washed three times with PBS solution. The FIs in the isolated organs were measured using Lago-X at excitation and emission wavelength of 360 nm and 490 nm, respectively.

For the injection of compound mixtures, ICR mice were injected intravenously with Umb and compound mixtures (weight ratio of other compound/Umb = 1) in injection buffer at an Umb dose of 80 mg/kg, and left for 2 min. After 2 min, the mice were euthanized, and organs were isolated and washed with PBS solution. Fluorescent images of each organ were analyzed using Lago-X at an excitation and emission wavelength of 360 nm and 490 nm, respectively. The total flux within a whole organ was quantitatively analyzed after subtracting background signals using the following formula: total flux in tissue from treated mice - total flux in tissue from untreated mice. *A. gigas* extract and single compounds (Byn, Ang, and Dec) were also injected into the mice tail vein at doses of 120 mg/kg (extract) and 40 mg/kg (single compound). After incubation for 15 min, the FI in each organ was monitored using Lago-X at an excitation/emission wavelength of 360/490 nm, respectively. To determine whether the blood-brain barrier (BBB) was disrupted by Umb or the compound mixtures, ICR mice were injected intravenously with freshly prepared Umb and Umb mixtures (other compound/Umb weight ratio of 1) at an Umb dose of 40 mg/kg. After incubation for 15 min, a 1% Eb solution in PBS was injected intravenously. After an additional 15 min of incubation, the mice were euthanized and fluorescent images of Eb in each tissue were acquired using an *in vivo* imaging system (IVIS) instrument (Caliper Life Sciences Lumina II, MA, USA) at an excitation and emission wavelength of 535 and 705 nm, respectively.

Umb mixtures (Byn/Umb, Dec/Umb, Del/Umb, Nod/Umb, and Ang/Umb) dissolved in DMSO were diluted with injection buffer at a final Umb concentration of 0.5 mg/ml, and then injected into ICR mice at an Umb dose of 4 mg/kg at different other compound/Umb weight ratios of 0, 1, and 20. After 2 min, the organs were collected and analyzed using Lago-X at an excitation and emission wavelength of 360 nm and 490 nm, respectively. The total flux in each organ was analyzed using the Lago-X software. To quantify the amount of Umb in different organs (brain, lung, and pancreas), Umb was extracted using ethyl acetate after the isolated organs were homogenized according to previous study (Kang et al., 2016a). Briefly, the organs were homogenized in PBS solution and the homogenate was then mixed with a solution of 10% SDS and ethyl acetate to give a volume ratio of homogenate:10% SDS:ethyl acetate of 1:0.5:5. After vortexing the mixture for 10 min, the sample was centrifuged at 12,000 rpm for 3 min. The supernatant was then collected and dried at room temperature. After the dried tissue extracts were re-dissolved in DMSO, the FIs in samples were measured at an excitation and emission wavelength of 325 and 495 nm using a fluorospectrophotometer (Molecular Devices, CA, USA). The FI of Umb in DMSO (0–500 ng/ml) served as standard for quantification.

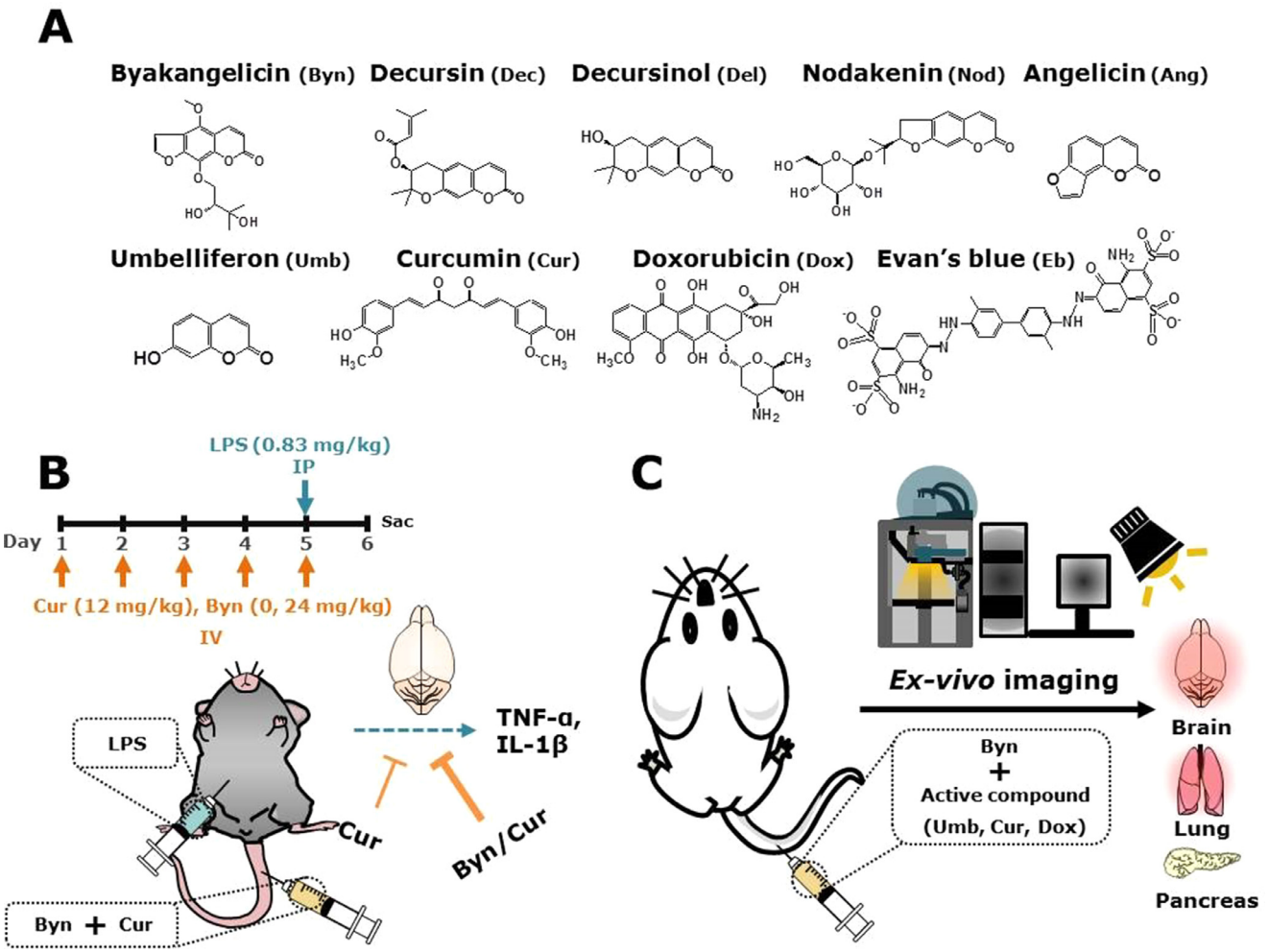

Fig. 1. (A) Chemical structures of six compounds derived from *Angelica gigas*: Byn, Dec, Del, Nod, Ang, and Umb, and the active compound Cur, Dox, and Eb. (B) Illustration of the experimental protocol used to assess neuro-inflammation. Mice were intravenously injected with buffer (Buffer), Cur, and Byn/Cur for 5 days. On the 5th day, 30 min after the last injection, LPS (0.83 mg/kg) was injected intraperitoneally. (C) Schematic illustration of the procedure used to examine the biodistribution of compound mixtures using *ex vivo* fluorescence images.

Ex vivo fluorescence imaging of Cur and Dox in brain

To measure the FI of Cur and Byn/Cur solutions, each sample was prepared in injection buffer at a Cur concentration of 1 μg/ml (at a weight ratio of Byn/Cur of 2). After samples were loaded into 96-well black plates, the FIs were analyzed using an *in vivo* imaging system at an excitation and emission wavelength of 430 and 509 nm, respectively.

Cur mixtures with other compounds, including Byn/Cur, Dec/Cur, and Ang/Cur, were prepared at various weight ratios (other compound/Cur weight ratios of 0, 20, and 50). Dox mixtures with other compounds, including Byn/Dox, Dec/Dox, and Nod/Dox, were also prepared at other compound/Dox weight ratios of 0, 5, and 10, respectively. For injection, the Cur and Dox mixtures in DMSO were mixed with kolliphor and PBS at 1.5:1.5:7.0 (volume ratio of DMSO: kolliphor: PBS), according to a previous study (Zhang et al., 2015). Freshly prepared Cur (1.6 mg/kg) and Dox (5 mg/kg) mixtures were injected intravenously into ICR mice, respectively. After incubation for 2 min, the brain and lung were isolated and washed with PBS solution. The fluorescent signal in each organ was analyzed using IVIS instrument at an excitation/emission wavelength of 430/509 nm for Cur, and at an excitation/emission wavelength of 465/583 nm for Dox, respectively. As a control, Eb was mixed with Byn at Byn/Eb weight ratios of 0, 0.5, 1, 2, 20, and 50. The Byn/Eb mixtures in injection buffer were intravenously administered at an Eb dose of 1.6 mg/kg. After 2 min, the mice were perfused with saline, the organs were collected and analyzed using IVIS instrument at excitation/emission wavelength of 535/705 nm.

LPS-induced neuro-inflammation model

A neuro-inflammation animal model was established, as previously described (Walker et al., 2013; Wang et al., 2014). C57/BL6 mice were randomly divided into four groups: a normal group treated with injection buffer (Control); a control group pre-treated with injection buffer before LPS injection (Buffer); a Cur group pre-treated with Cur before LPS injection (Cur); and a Byn/Cur group pre-treated with Byn/Cur before LPS injection (Byn/Cur). All solutions were prepared fresh on the day of administration. The schedule for Cur injection was slightly modified based on a previous study (Kawamoto et al., 2013; Wang et al., 2014). For pre-treatment, a solution of Cur and Byn/Cur in injection buffer was injected into the tail vein once per a day at a Cur dose of 12 mg/kg and Byn doses of 0 and 24 mg/kg for 5 days, respectively. Thirty minutes after injection on the 5th day, the mice in groups of Buffer, Cur, and Byn/Cur were injected intraperitoneally with LPS (0.83 mg/kg). After 24 h of LPS injection, the mice were anesthetized with isoflurane and sera were collected from mice. After perfusion, the brains were collected and cut into half. The brains in left-hand side were used to prepare a homogenate, whereas brains in right-hand side were used for brain imaging. For confocal imaging, the right-hand brain sections were fixed in 3.7% formaldehyde in PBS solution for 48 h, and then dehydrated in 15 and 30% (w/v) sucrose in PBS solution. The samples were frozen in optimum cutting temperature (OCT) and a

coronal section with a width of 10 μm was made using a cryostat (CM1860, Leica Co., Wetzlar, Germany). After the samples were stained with DAPI, the FIs of Cur and DAPI in each tissue slice were observed using fluorescence microscopy (Olympus, Shinjuku, Japan) and confocal microscopy (LSM 800, Carl Zeiss, Oberkochen, Germany), respectively.

Determination of cytokine levels in brain lysates and sera

To measure the levels of pro-inflammatory cytokines in the brain, brains were homogenized in PBS solution. After centrifugation at 13,000 rpm at 4 °C for 10 min, supernatants were collected and stored at −80 °C until used. To prepare serum, the isolated blood was centrifuged at 2000 × *g* for 15 min. The amount of protein in each sample was quantified using a BCA protein assay kit according to the manufacturer's protocol. The amounts of TNF-α and IL-1β in the each brain homogenate and serum were determined using mouse ELISA kits. The absorbance was measured at 450 nm using a microplate reader (SpectraMAX, Molecular Devices, Sunnyvale, CA, USA).

Results

Biodistribution of Umb via ex vivo fluorescence imaging

Fig. 1A shows the chemical structures of six compounds derived from *A. gigas*. Among these compounds, Umb, a coumarin-based compound, was selected as a tracing compound due to its strong absorbance at a wavelength of 325 nm and its fluorescence at a wavelength of 495 nm (Simkovitch et al., 2016; Vasconcelos et al., 2009). Other bioactive compounds, Cur and Dox, were also examined to monitor *in vivo* biodistribution. As a control dye, Eb was also administered to mice to examine its brain localization. After these single compounds and mixture of these compounds were injected into normal mice and a neuro-inflammatory mouse model, their biodistribution was determined in isolated organs. In particular, the biodistribution of active compounds (Umb, Cur, and Dox) in each organ was directly visualized using an *ex vivo* fluorescence imaging instrument without the need for time-consuming and complicated extraction processes, as shown in Fig. 1C. The neuro-inflammation mouse model was established by the intraperitoneal injection of LPS (Walker et al., 2013; Wang et al., 2014). To assess the anti-inflammatory effects of Cur and the Byn/Cur mixtures, these agents were intravenously injected five times into mice (Fig. 1B). After administration, the accumulation of Cur in the brain and its anti-inflammatory responses were examined by fluorescence microscopy and by ELISA of cytokines, respectively.

Fig. 2A shows the fluorescence images of single compounds and other compound/Umb mixtures in aqueous solution. A noticeable fluorescence signal was only observed in the presence of Umb (Fig. 2A). The normalized FIs of Umb, Byn/Umb, Dec/Umb, and Ang/Umb were 100.9 ± 5.8, 101.3 ± 3.3, 97.3 ± 8.8, and 102.9 ± 6.0, indicating that the other compounds had negligible effects on Umb fluorescence. After intravenous injection of Umb at a dose of 160 or 320 mg/kg in mice, the organ distribution of Umb was monitored by fluorescence imaging. Strong fluorescence signals were observed in the brain, lung, and pancreas (Fig. 2B). It is well known that Umb has therapeutic effects in diabetes and neurodegenerative diseases, which are correlated to the biodistribution of Umb (Naowaboot et al., 2015; Ramu et al., 2016; Subramaniam and Ellis, 2013; Wang et al., 2015). To examine whether the biodistribution of Umb could be changed by co-administration with other compounds from *A. gigas*, Umb mixtures with Byn, Dec, and Ang were injected intravenously into mice. The localization of Umb in each organ was then observed by fluorescence imaging. After 2 min, much stronger Umb fluorescence signals were observed in the brain and lung following the administration of the Byn/Umb mixture than those with the other mixtures (Fig. 2C). Significantly reduced fluorescence signals in the pancreas were observed in mice treated with the Byn/Umb and Ang/Umb mixtures. However, as shown in Fig. S1A, Byn, Dec, and Ang alone showed negligible fluorescence signals in any organs after intravenous injection. The fluorescence signals in each organ were also analyzed quantitatively after extraction. The levels of Umb in the brain, lung, and pancreas were noticeably reduced following the administration of Umb with another compound (Fig. 2D). The normalized FIs of Umb alone, Byn/Umb, Dec/Umb, and Ang/Umb were 382.1 ± 69.0, 630.5 ± 104.4, 363.8 ± 104.6, and 503.2 ± 64.0 ($\times 10^{-3}$) in the brain, and 177.4 ± 23.8, 132.3 ± 4.5, 163.4 ± 36.5, and 344.3 ± 272.9 ($\times 10^{-3}$) in the lung. The greatest accumulation of Umb in both the brain and lung occurred after administration of Umb with Byn. As shown in Fig. S1B, FIs of Byn, Dec, and Ang were negligible after extraction from each organ. To examine whether the increased accumulation of Umb that was observed was mediated by disruption of the BBB following the administration of compound mixtures or not, Eb was also administered after compound treatment. Fig. S1C clearly shows that there was poor accumulation of Eb in the brain. This result clearly indicates that the BBB remained intact after the administration of the compound mixtures.

Accumulation of Byn/Umb mixtures in brain

The accumulation of Umb in the brain was also assessed as increasing other compound/Umb weight ratios. After intravenous injection of mice with Umb and Umb mixtures (Byn/Umb, Dec/Umb, Del/Umb, Nod/Umb, and Ang/Umb) at an Umb dose of 4 mg/kg, the localization of Umb in each isolated organ was observed by fluorescence imaging (weight ratio of other compound/Umb of 20). As shown in Fig. 3A, Umb FI was significantly elevated in the brain and lung after treatment with the Byn/Umb mixture. However, there was no noticeable increase of FI in pancreas following the administration of Byn/Umb. Nod/Umb showed a higher accumulation of Umb in pancreas, compared with other compound mixtures. The FIs in each organ were also quantitatively analyzed. Fig. 3B shows that the normalized FIs of Umb in each organ (brain, lung, and pancreas) were 8.9 ± 4.7, 8.1 ± 9.1, and 8.2 ± 6.2 ($\times 10^{-3}$), respectively. The FIs of Byn/Umb (at a weight ratio of other compound/Umb of 20) in the brain and lung were 37.4 ± 0.1 and 58.0 ± 29.5 ($\times 10^{-3}$), respectively. The FIs in the brain and lung of mice treated with Byn/Umb were 4.2-fold and 7.2-fold greater, respectively than in the brain and lung of mice treated with Umb alone. To confirm whether the Umb levels in organs identified by *ex vivo* fluorescence monitoring correlated with conventional analytic methods, the physical amount of Umb was assessed using a fluorospectrometer after its extraction from each organ. Fig. 3C shows the relative FI in tissue lysates extracted from each organ using ethyl acetate. As expected, the brain and lung from mice injected with Byn/Umb showed a much larger amount of Umb compared with mice injected with Umb alone (Fig. 3C). However, the amount of Umb extracted from the brains and lungs of mice treated with Ang/Umb was similar to that extracted from the brains and lungs of mice injected with Umb alone, which was not consistent with the *ex vivo* imaging results. This could be attributed to the instability of Umb during the complicated extraction process. Mixtures of Byn and Nod with Umb showed significantly increased Umb levels in the brain and pancreas, respectively. This result was correlated well with the *ex vivo* monitoring in Fig. 3B. The Byn/Umb mixtures at Byn/Umb weight ratio of 20 resulted in a 2.4 ± 0.1-fold elevation of Umb accumulation in the brain, compared to Umb only.

Biodistribution of Cur and Dox via ex vivo fluorescence imaging

To investigate whether Byn could modulate the biodistribution of different types of active compounds, Cur and Dox mixtures with Byn were administered to mice intravenously. Cur is a well-known polyphenol, found in turmeric, for its therapeutic effect in neuro-inflammatory diseases and Alzheimer's disease (Mishra and Palanivelu, 2008). As shown in Fig. S2A, as the concentration of Cur

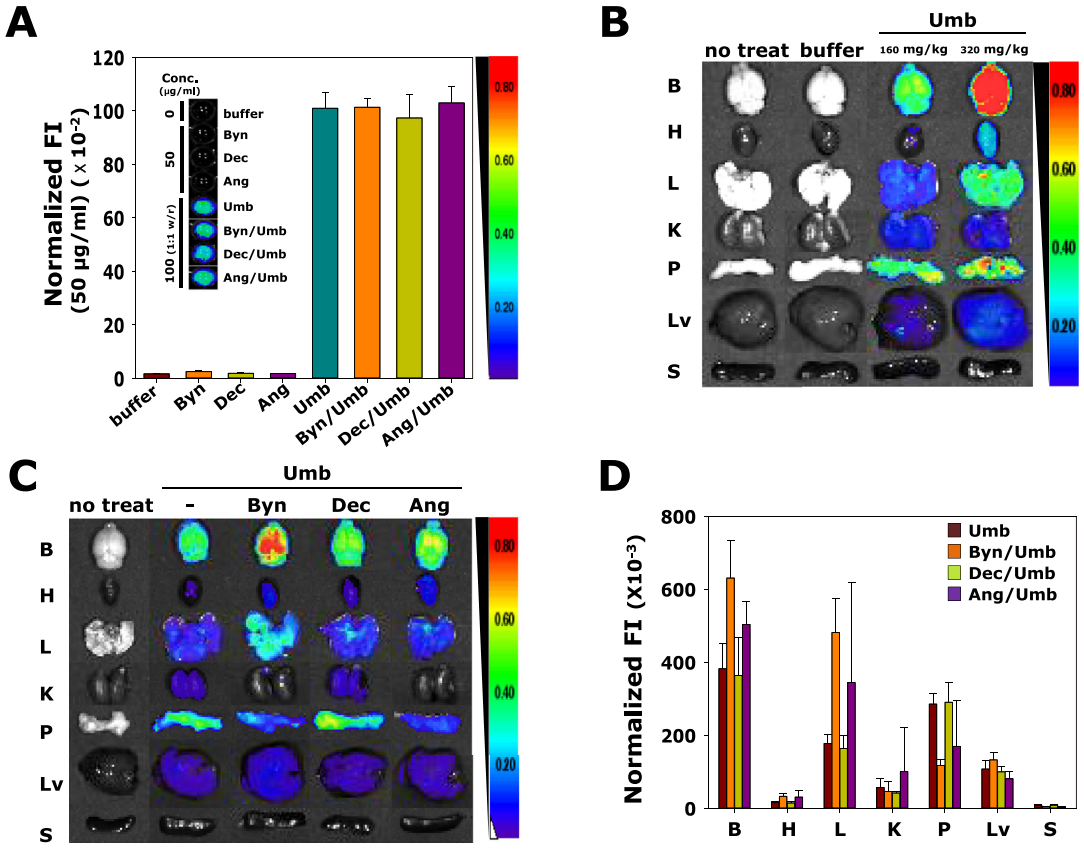

Fig. 2. (A) Fluorescence images of single compounds or compound mixtures were analyzed by Lago-X at excitation and emission wavelength of 360 and 490 nm, respectively. (B) *Ex vivo* fluorescence images from each organ after intravenous administration of a Umb solution (160 and 320 mg/kg). B, Brain; H, Heart; L, Lung; K, Kidney; P, Pancreas; Lv Liver; S, Spleen. (C) *Ex vivo* fluorescence images and (D) quantitative analysis of each organ after administration of Umb alone and Umb mixtures (1:1 wt ratio) at 80 mg/kg intravenously, and incubation for 2 min. B, brain; L, lung; P, pancreas.

increased, the fluorescent signal of Cur became strong accordingly. A Cur mixture with Byn (Byn/Cur) showed a similar FI to Cur alone, which indicates that the amount of Cur in tissues treated with Cur and Byn/Cur mixtures could be measured by FI of Cur in solution, respectively (Fig. S2B). Dox is a representative anticancer drug that is used to treat diverse types of tumors including neuroblastoma (MacDiarmid et al., 2016). However, poor penetration of Dox across BBB has limited its anticancer effects for brain tumors (Rousselle et al., 2000; Seol et al., 2014). Accordingly, development of promising delivery systems for Dox to brain has been greatly paid attention. Both Cur and Dox can be fluorescently excited by exterior light, which could be easily monitored after their administration *in vivo* (Kang et al., 2016b; Motlagh et al., 2016). Fig. 4A shows the fluorescence signals of Cur in the brain and lung after the administration of the Cur mixtures (Byn/Cur, Dec/Cur, and Ang/Cur). The Byn/Cur mixture showed a significantly strong FI in the brain and lung, compared to Cur only and other compound mixtures. The FI in each organ was also quantitatively analyzed, as shown in Fig. 4B. The normalized FIs for Cur, Byn/Cur, Dec/Cur, and Ang/Cur (weight ratio of other compound/Cur = 50) in the brain were 3.6 ± 1.2, 8.3 ± 2.1, 5.8 ± 1.7, and 7.5 ± 1.0. In addition, the normalized FIs for Cur, Byn/Cur, Dec/Cur, and Ang/Cur (weight ratio of other compound/Cur = 50) in the lung were 6.2 ± 2.7, 46.5 ± 2.0, 6.7 ± 2.7, and 18.7 ± 17.1, respectively. Interestingly, a more than 7-fold accumulation of Cur was observed in lung with the Byn/Cur mixture, compared to the Cur only. In our previous study, Cur bio-distribution determined by *ex vivo* fluorescence imaging was greatly correlated with that by mass spectrometry analysis of extracted Cur from tissues (Kang et al., 2016a). Accordingly, strong fluorescence intensities of Cur in tissues might indicate actual accumulation of Cur in tissues. However, it is necessary to examine Cur distribution at diverse time intervals to elucidate the maximal accumulation of Cur in different tissues (Wei et al., 2017; Zhang et al., 2019). Fig. 4C shows the accumulation of Dox in three different organs. As expected, Dox mixtures with Byn exhibited highest Dox accumulation in the brain among other compound mixtures. The normalized FIs for Dox, Byn/Dox, Dec/Dox, and Nod/Dox (weight ratio of other compound/Dox = 10) in the brain were 2.6 ± 0.7, 15.0 ± 6.8, 9.0 ± 6.5, and 2.9 ± 0.6, respectively (Fig. 4D). Taken together, Byn mixtures with Umb, Cur, and Dox greatly elevated their accumulation in the brain by 4.2-folds, 2.3-folds, and 5.7-folds, respectively, compared to their injection without Byn. To examine whether Byn could facilitate the penetration of Eb, Eb was mixed with Byn, and the mixture was used to treat mice. Fig. S3 shows that the FIs of Eb in the brain, lung, and pancreas after administration of Byn/Eb mixtures were similar to those after treatment with Eb alone. This result clearly demonstrates that Byn enhances the brain accumulation of selected active compounds without disruption of the BBB.

Brain accumulation of Cur in of LPS-induced inflammation model

To examine the localization of Cur in an LPS-induced mouse inflammation model, Cur and Byn/Cur were administered intravenously to the mice for 5 days. After administration of Cur and Byn/Cur on the 5th day, LPS was also injected intraperitoneally to the mice. After 24 h, the brain was isolated and fixed for the preparation of coronal sections. Accumulation of Cur in the coronal sections was seen in the cerebrum (Fig. 5A) using fluorescence microscopy and in the hippocampus (Fig. 5B) using confocal microscopy. A significant enhancement of Cur accumulation was observed in the cerebrum after Byn/Cur treatment, compared to Cur only. A strong green fluorescence signal was observed

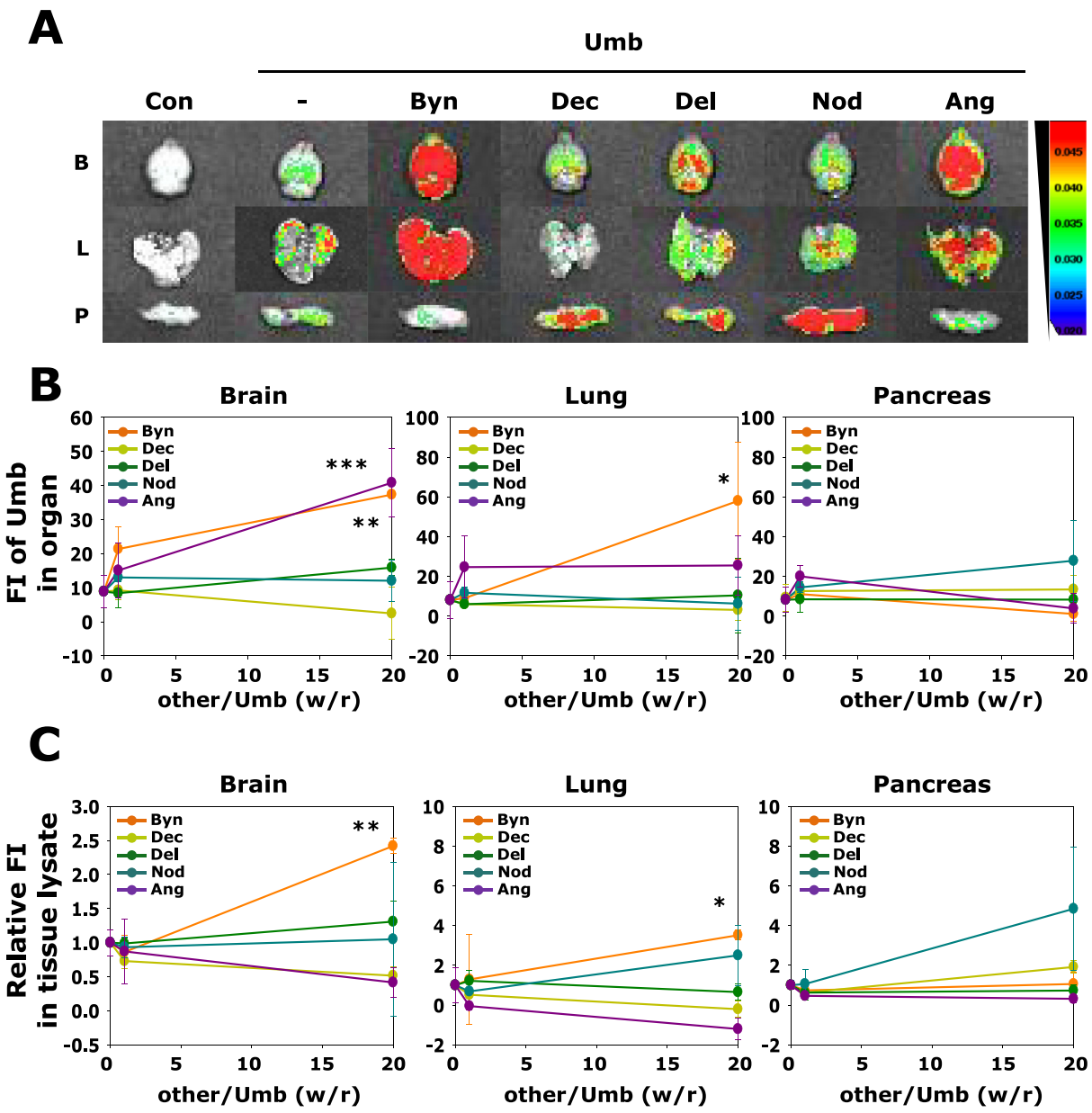

Fig. 3. (A) *Ex vivo* fluorescence images of Umb or Umb mixtures (1:20, weight ratio) analyzed by Lago-X at excitation/emission wavelength of 360/490 nm, respectively. (B) quantitative analysis of each organ after administration of Umb alone and Umb mixtures at 4 mg/kg intravenously and incubation for 2 min. (C) Quantification of Umb using a fluorospectrometer after extraction from the brain, lung, pancreas following the intravenous administration of Umb mixtures and incubation for 2 min. B, brain; L, lung; P, pancreas.

not only in the cerebrum but also in the hippocampus region. Taken together, these results indicate that Byn allowed excellent accumulation of Cur in the cerebrum and hippocampus in an LPS-induced inflammation model.

Anti-inflammatory effect of Byn/Cur in the LPS-induced inflammation model

To investigate anti-inflammatory effects of Byn/Cur in the LPS-induced inflammation model, the level of cytokines in brain homogenates and serum were measured by ELISA after administration of Cur and Byn/Cur. The amounts of TNF-α in the Control, Buffer, Cur, and Byn/Cur groups were 14.5 ± 1.4, 25.6 ± 1.6, 14.5 ± 1.3, and 11.2 ± 2.7 pg/mg, respectively (Fig. 6A). The levels of TNF-α in the brain homogenate were slightly decreased in the Byn/Cur group, compared with the Cur group. In addition, significant differences in the level of IL-1β were observed in the Cur and Byn/Cur groups. The amounts of IL-1β in the Control, Buffer, Cur, and Byn/Cur groups were 1.8 ± 1.1, 7.6 ± 1.2, 3.6 ± 0.8, and 2.3 ± 0.7 pg/mg, respectively (Fig. 6B). To compare the systemic anti-inflammatory effect of Cur and Byn/Cur, the levels of TNF-α in sera were analyzed, as shown in Fig. 6C. After 24 h of LPS administration, the level of TNF-α in sera was 30.1 ± 4.5 pg/ml. However, the levels of TNF-α in sera from the Cur and Byn/Cur groups were reduced to 23.4 ± 2.3 and 4.5 ± 4.5 pg/ml, respectively. It should be noted that TNF-α levels in the Byn/Cur group were almost similar to those in mice without LPS injection (Control). This result clearly shows that the enhanced accumulation of Byn/Cur allows for a successful anti-inflammatory effects on mouse neuro-inflammation model.

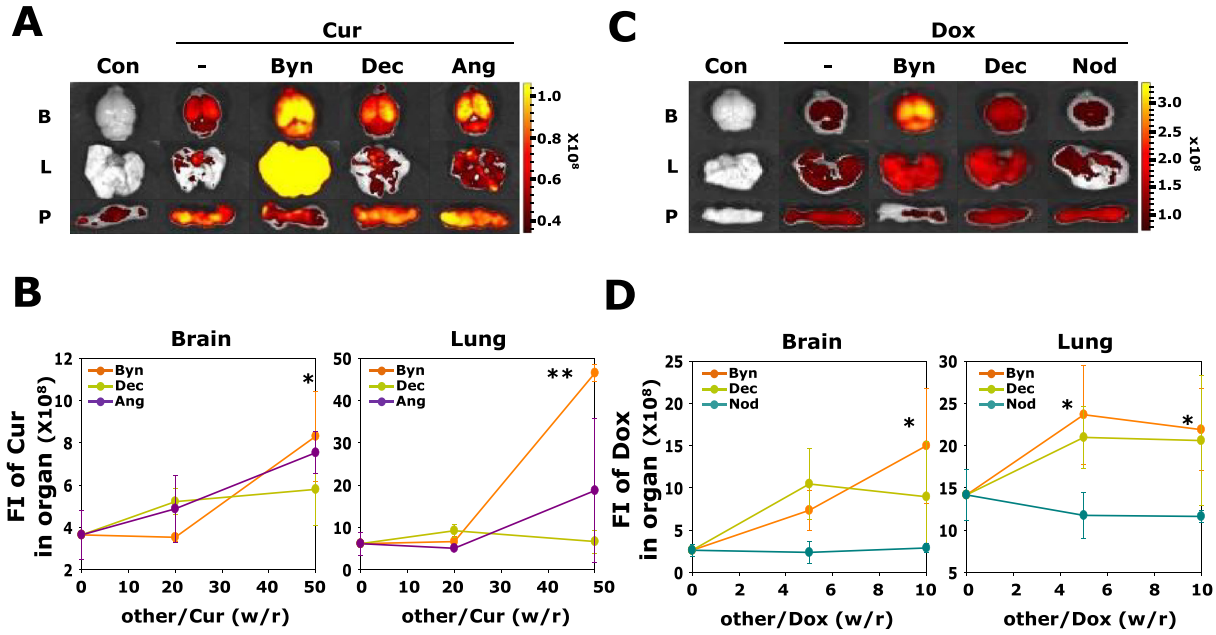

Fig. 4. (A) *Ex vivo* fluorescence images of brain, lung, pancreas after administration of Cur or Cur mixtures (1:50, weight ratio) analyzed by IVIS at excitation/emission wavelength of 430/509 nm, respectively. (B) Quantitative analysis of brain and lung after administration Cur (1.6 mg/kg) and incubation for 2 min. (C) *Ex vivo* fluorescence images of brain, lung, pancreas after the administration of Dox or Dox mixtures (1:10, weight ratio) analyzed by IVIS at excitation/emission wavelength of 535/705 nm, respectively. (D) Quantitative analysis of brain and lung after administration of Dox (5 mg/kg) and incubation for 2 min. B, brain; L, lung; P, pancreas.

Discussion

Although an efficient brain delivery system is necessary and important for the development of treatments for neurodegenerative diseases, promising strategies remain limited (Dong, 2018; Patel and Patel, 2017; Scherrmann, 2002). As a promising strategy to overcome the current challenges, in this study, we demonstrated the ability of Byn as a modulator for the brain localization of active compounds *in vivo*. Byn could successfully enhance the brain accumulation of different polyphenols and drugs which was monitored using *ex vivo* fluorescent imaging. Because Eb delivery to the brain was not enhanced by Byn, the elevated localization of the different polyphenols and drugs was caused not by a disruption of the BBB. However, the exact mechanism for this improved brain accumulation of active compounds by Byn remains to be determined. In our previous study, Byn resulted in elevated intracellular uptake of Umb into MCF-7 breast cancer cells while there were no noticeable effects on P-gp inhibition for cancer cells and enhanced stability of Umb in liver homogenates (Kang et al., 2019). Further detailed mechanisms of Byn for the brain accumulation of active compounds should be examined for neurons and brain endothelial cells. Previous studies have reported that the expression levels of P-gp on the luminal side of the BBB epithelia can limit the accumulation of drugs after their administration (Syvanen and Eriksson, 2013; Trezise et al., 1992). Accordingly, it is necessary to examine the expression levels of proteins related to BBB penetration after Byn treatment in next study.

The elevated accumulation of Byn/Cur in the cerebrum and hippocampus greatly reduced the levels of pro-inflammatory cytokines.

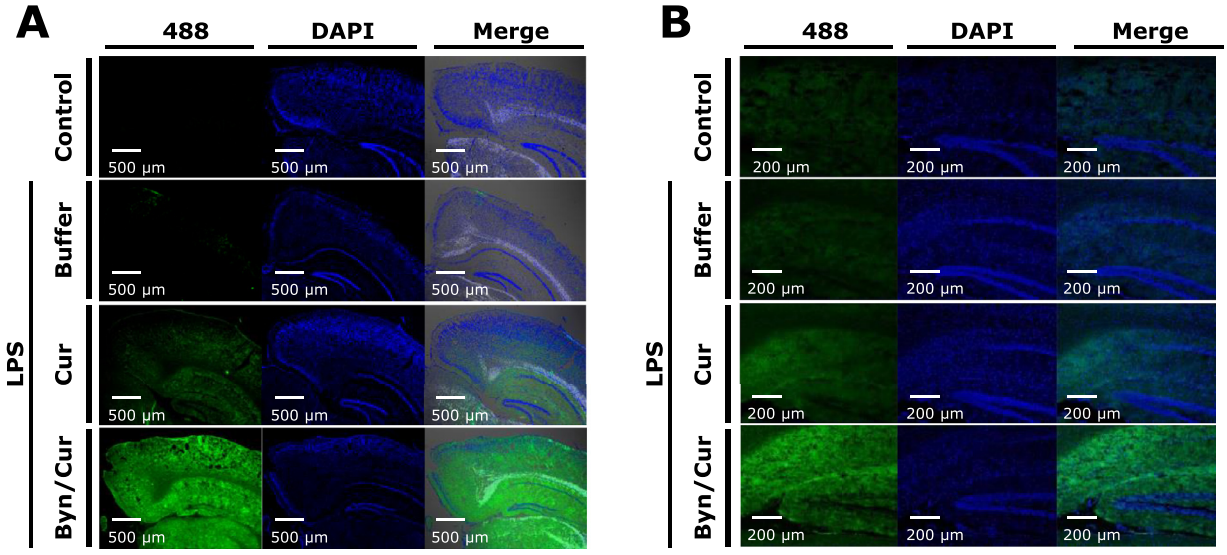

Fig. 5. (A) Fluorescence microscopy images of the cerebrum. (B) Confocal microscopy images of the hippocampus treated with Cur or Byn/Cur.

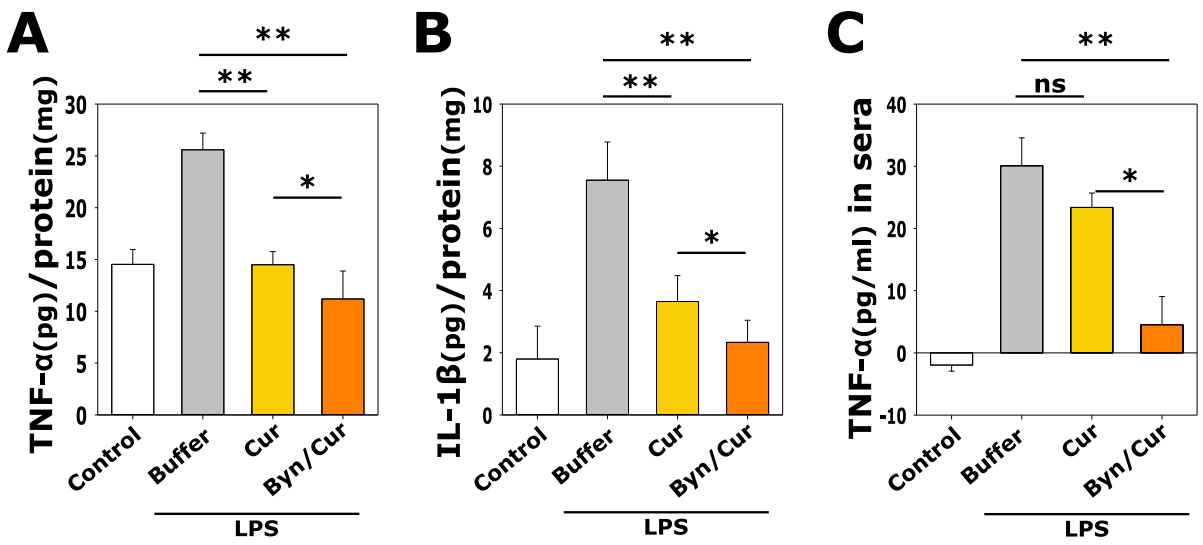

Fig. 6. Amounts of (A) TNF-α (B) IL-1β in brain lysate and (C) TNF-α in sera measured via ELISA. $*p < 0.05$, $**p < 0.01$, $***p < 0.001$.

Not only brain inflammation was reduced, but there was also a significant alleviation of systemic inflammation in serum following treatment with Byn/Cur. LPS-induced inflammation is induced by activation of the NF-κB pathway and the formation of the NLRP3 inflammasome as a result of the deubiquitination of NLRP3 (Chow et al., 1999; Guo et al., 2015; Liu et al., 2017). Based on the intracellular functions of Cur, the improved brain accumulation in mice treated with Byn/Cur might result in increased inhibition of the NF-κB pathway and decreased levels of pro-inflammatory cytokines (TNF-α and IL-1β) (Aggarwal et al., 2013; Sun et al., 2018; Yin et al., 2018). In a previous study, it was shown that Cur can cross the BBB and attenuate both neuro-inflammatory and neurodegenerative diseases (Figueira et al., 2017; Mishra and Palanivelu, 2008). Here, we developed a novel approach to improve the brain accumulation of Cur simply by mixing Cur with Byn. In particular, considering that neuro-inflammation is closely related to depression and neurodegenerative diseases (Alzheimer's disease, Parkinson's disease, Huntington's disease, and multiple sclerosis), a Byn-mediated brain delivery strategy could be harnessed for the treatment of diverse neuronal diseases (Singhal et al., 2014). It should be noted that the superior brain accumulation was shown not only for Cur but also for other active compounds. Thus, the efficient brain accumulation of therapeutic molecules by Byn could enhance the diverse therapeutic effects by other drugs related to brain diseases. In addition, it might be also interesting to examine whether Byn could improve the localization of nutrients and nanoparticles.

Lastly, studies regarding the roles of candidate molecules in other natural extracts *e.g.* modulators of biodistribution could provide us with many clues to understand synergistic biological activity of natural extracts over single active compounds. Our *ex vivo* monitoring strategy could be applied to other types of natural compounds to elucidate the advantages of combinatorial treatment and optimize compound mixtures for their synergistic bio-distribution and biological effects in brain, which can play a major role in improving clinical efficacy and the therapeutic effects of compounds.

Conclusion

In this study, the role of Byn was evaluated as a modulator for brain accumulation of active compounds *in vivo* models through easy and direct *ex vivo* fluorescence imaging. Byn improved the accumulation of numerous active compounds *e.g.* polyphenols and anticancer drugs (Umb, Cur, and Dox) in the brain after intravenous injection. However, other components derived from *A. gigas,* including Ang, Byl, and Dec showed negligible effects on the brain accumulation of active compounds. In a neuronal inflammation-induced mouse model, the anti-inflammatory effects of Byn/Cur were significantly greater than Cur alone in terms of reduction of the levels of pro-inflammatory cytokines (TNF-α and IL-β) in the brain. Thus, Byn could serve as a modulator of the brain distribution of diverse active compounds to allow their improved brain accumulation and enhanced therapeutic effects.

Acknowledgments

This study was supported by a grant (NRF-2017R1A2B4001964) though the National Research Foundation (NRF) funded by the Ministry of Education, Science and Technology; and the Agri-Bio Industry Technology Development Program (316028-3), Korea Institute of Planning and Evaluation for Technology in Food, Agriculture, Forestry and Fisheries (IPET), Republic of Korea.

Conflict of interest

The authors have declared no conflict of interest

References

Aggarwal, B.B., Gupta, S.C., Sung, B., 2013. Curcumin: an orally bioavailable blocker of TNF and other pro-inflammatory biomarkers. Br. J. Pharmacol. 169, 1672–1692.
Bi, X., Yuan, Z., Qu, B., Zhou, H., Liu, Z., Xie, Y., 2019. Piperine enhances the bioavailability of silybin via inhibition of efflux transporters BCRP and MRP2. Phytomedicine 54, 98–108.
Chow, J.C., Young, D.W., Golenbock, D.T., Christ, W.J., Gusovsky, F., 1999. Toll-like receptor-4 mediates lipopolysaccharide-induced signal transduction. J. Biol. Chem. 274, 10689–10692.
Dong, X., 2018. Current strategies for brain drug delivery. Theranostics 8, 1481–1493.
Fantini, M., Benvenuto, M., Masuelli, L., Frajese, G.V., Tresoldi, I., Modesti, A., Bei, R., 2015. *In vitro* and *in vivo* antitumoral effects of combinations of polyphenols, or polyphenols and anticancer drugs: perspectives on cancer treatment. Int. J. Mol. Sci. 16, 9236–9282.
Figueira, I., Garcia, G., Pimpao, R.C., Terrasso, A.P., Costa, I., Almeida, A.F., Tavares, L., Pais, T.F., Pinto, P., Ventura, M.R., Filipe, A., McDougall, G.J., Stewart, D., Kim, K.S., Palmela, I., Brites, D., Brito, M.A., Brito, C., Santos, C.N., 2017. Polyphenols journey through blood-brain barrier towards neuronal protection. Sci. Rep. 7, 11456.
Guo, H., Callaway, J.B., Ting, J.P., 2015. Inflammasomes: mechanism of action, role in disease, and therapeutics. Nat. Med. 21, 677–687.
Hsu, P.W., Shia, C.S., Lin, S.P., Chao, P.D., Juang, S.H., Hou, Y.C., 2013. Potential risk of mulberry-drug interaction: modulation on P-glycoprotein and cytochrome P450 3A. J. Agric. Food Chem. 61, 4464–4469.
Kan, W.L., Cho, C.H., Rudd, J.A., Lin, G., 2008. Study of the anti-proliferative effects and synergy of phthalides from Angelica sinensis on colon cancer cells. J. Ethnopharmacol. 120, 36–43.
Kang, Y.Y., Choi, I., Chong, Y., Yeo, W.S., Mok, H., 2016a. Complementary analysis of curcumin biodistribution using optical fluorescence imaging and mass spectrometry.

Appl. Biol. Chem. 59, 291–295.
Kang, Y.Y., Jung, H., Yu, G., Chong, Y., Mok, H., 2016b. Complexation of curcumin with 2-aminoethyl diphenyl borate and implications for spatiotemporal fluorescence monitoring. Int. J. Pharm. 515 (, 1–2), 669–676.
Kang, Y.Y., Kim, J.Y., Song, J., Mok, H., 2019. Enhanced intracellular uptake and stability of umbelliferone in compound mixtures from Angelica gigas *in vitro*. J. Pharmacol. Sci. https://doi.org/10.1016/j.jphs.2019.02.010. in press.
Kawamoto, E.M., Scavone, C., Mattson, M.P., Camandola, S., 2013. Curcumin requires tumor necrosis factor alpha signaling to alleviate cognitive impairment elicited by lipopolysaccharide. Neurosignals 21, 75–88.
Kim, H.B., Hwang, E.S., Choi, G.Y., Lee, S., Park, T.S., Lee, C.W., Lee, E.S., Kim, Y.C., Kim, S.S., Lee, S.O., Park, J.H., 2016. ESP-102, a combined herbal extract of Angelica gigas, saururus chinensis, and schisandra chinensis, changes synaptic plasticity and attenuates scopolamine-induced memory impairment in rat hippocampus tissue. Evid.-based Complement. Altern. Med. 2016, 8793095.
Lee, H.J., Lee, E.O., Lee, J.H., Lee, K.S., Kim, K.H., Kim, S.H., Lu, J., 2009. *In vivo* anticancer activity of Korean Angelica gigas and its major pyranocoumarin decursin. Am. J. Chin. Med. 37, 127–142.
Liu, T., Zhang, L., Joo, D., Sun, S.C., 2017. NF-kappaB signaling in inflammation. Signal Transduct. Target. Ther. 2, e17023.
MacDiarmid, J.A., Langova, V., Bailey, D., Pattison, S.T., Pattison, S.L., Christensen, N., Armstrong, L.R., Brahmbhatt, V.N., Smolarczyk, K., Harrison, M.T., Costa, M., Mugridge, N.B., Sedliarou, I., Grimes, N.A., Kiss, D.L., Stillman, B., Hann, C.L., Gallia, G.L., Graham, R.M., Brahmbhatt, H., 2016. Targeted doxorubicin delivery to brain tumors via minicells: proof of principle using dogs with spontaneously occurring tumors as a model. PLoS One 11, e0151832.
Mishra, S., Palanivelu, K., 2008. The effect of curcumin (turmeric) on Alzheimer's disease: an overview. Ann. Indian Acad. Neurol. 11, 13–19.
Motlagh, N.S.H., Parvin, P., Ghasemi, F., Atyabi, F., 2016. Fluorescence properties of several chemotherapy drugs: doxorubicin, paclitaxel and bleomycin. Biomed. Opt. Express 7, 2400–2406.
Naowaboot, J., Somparn, N., Saentaweesuk, S., Pannangpetch, P., 2015. Umbelliferone improves an impaired glucose and lipid metabolism in high-fat diet/streptozotocin-induced type 2 diabetic rats. Phytother. Res. 29, 1388–1395.
Oh, T.W., Park, K.H., Jung, H.W., Park, Y.K., 2015a. Neuroprotective effect of the hairy root extract of Angelica gigas NAKAI on transient focal cerebral ischemia in rats through the regulation of angiogenesis. BMC Complement. Altern. Med. 15, 101.
Oh, T.W., Park, K.H., Jung, H.W., Park, Y.K., 2015b. Neuroprotective effect of the hairy root extract of Angelica gigas NAKAI on transient focal cerebral ischemia in rats through the regulation of angiogenesis. BMC Complement. Altern. Med. 15.
Patel, M.M., Patel, B.M., 2017. Crossing the Blood-Brain Barrier: recent Advances in Drug Delivery to the Brain. CNS Drugs 31, 109–133.
Ramu, R., Shirahatti, P.S., Swamy, S.N., Zameer, F., Lakkappa Dhananjaya, B., Prasad, M.N.N., 2016. Assessment of In Vivo Antidiabetic Properties of Umbelliferone and Lupeol Constituents of Banana (Musa sp. var. Nanjangud Rasa Bale) Flower in Hyperglycaemic Rodent Model. PLoS One 11, e0151135.
Rousselle, C., Clair, P., Lefauconnier, J.M., Kaczorek, M., Scherrmann, J.M., Temsamani, J., 2000. New advances in the transport of doxorubicin through the blood-brain barrier by a peptide vector-mediated strategy. Mol. Pharmacol. 57, 679–686.
Rubio, L., Motilva, M.J., Romero, M.P., 2013. Recent advances in biologically active compounds in herbs and spices: a review of the most effective antioxidant and anti-inflammatory active principles. Crit. Rev. Food Sci. Nutr. 53, 943–953.
Sarker, S.D., Nahar, L., 2004. Natural medicine: the genus Angelica. Curr. Med. Chem. 11, 1479–1500.
Scherrmann, J.M., 2002. Drug delivery to brain via the blood-brain barrier. Vasc. Pharmacol. 38, 349–354.
Seol, H.S., Akiyama, Y., Shimada, S., Lee, H.J., Kim, T.I., Chun, S.M., Singh, S.R., Jang, S.J., 2014. Epigenetic silencing of microRNA-373 to epithelial-mesenchymal transition in non-small cell lung cancer through IRAK2 and LAMP1 axes. Cancer Lett. 353, 232–241.
Simkovitch, R., Pinto da Silva, L., Esteves da Silva, J.C., Huppert, D., 2016. Comparison of the photoprotolytic processes of three 7-hydroxycoumarins. J. Phys. Chem. B 120, 10297–10310.
Singhal, G., Jaehne, E.J., Corrigan, F., Toben, C., Baune, B.T., 2014. Inflammasomes in neuroinflammation and changes in brain function: a focused review. Front. Neurosci. 8, 315.
Sowndhararajan, K., Kim, S., 2017. Neuroprotective and cognitive enhancement potentials of Angelica gigas Nakai Root: a review. Sci. Pharm. 85, 21.
Subramaniam, S.R., Ellis, E.M., 2013. Neuroprotective effects of umbelliferone and esculetin in a mouse model of Parkinson's disease. J. Neurosci. Res. 91, 453–461.
Sun, J., Chen, F., Braun, C., Zhou, Y.Q., Rittner, H., Tian, Y.K., Cai, X.Y., Ye, D.W., 2018. Role of curcumin in the management of pathological pain. Phytomedicine 48, 129–140.
Syvanen, S., Eriksson, J., 2013. Advances in PET imaging of P-glycoprotein function at the blood-brain barrier. ACS Chem. Neurosci. 4, 225–237.
Trezise, A.E., Romano, P.R., Gill, D.R., Hyde, S.C., Sepulveda, F.V., Buchwald, M., Higgins, C.F., 1992. The multidrug resistance and cystic fibrosis genes have complementary patterns of epithelial expression. EMBO J. 11, 4291–4303.
Vasconcelos, J.F., Teixeira, M.M., Barbosa-Filho, J.M., Agra, M.F., Nunes, X.P., Giulietti, A.M., Ribeiro-Dos-Santos, R., Soares, M.B., 2009. Effects of umbelliferone in a murine model of allergic airway inflammation. Eur. J. Pharmacol. 609, 126–131.
Walker, A.K., Budac, D.P., Bisulco, S., Lee, A.W., Smith, R.A., Beenders, B., Kelley, K.W., Dantzer, R., 2013. NMDA receptor blockade by ketamine abrogates lipopolysaccharide-induced depressive-like behavior in C57BL/6J mice. Neuropsychopharmacol 38, 1609–1616.
Wang, X., Li, R., Fu, Q., Ma, S., 2015. Umbelliferone ameliorates cerebral ischemia-reperfusion injury via upregulating the PPAR gamma expression and suppressing TXNIP/NLRP3 inflammasome. Neurosci. Lett. 600, 182–187.
Wang, Z., Zhang, Q., Yuan, L., Wang, S., Liu, L., Yang, X., Li, G., Liu, D., 2014. The effects of curcumin on depressive-like behavior in mice after lipopolysaccharide administration. Behav. Brain Res. 274, 282–290.
Wei, Y., Liang, J., Zheng, X., Pi, C., Liu, H., Yang, H., Zou, Y., Ye, Y., Zhao, L., 2017. Lung-targeting drug delivery system of baicalin-loaded nanoliposomes: development, biodistribution in rabbits, and pharmacodynamics in nude mice bearing orthotopic human lung cancer. Int. J. Nanomed. 12, 251–261.
Xiao, J., Kai, G., 2012. A review of dietary polyphenol-plasma protein interactions: characterization, influence on the bioactivity, and structure-affinity relationship. Crit. Rev. Food Sci. Nutr. 52, 85–101.
Yan, J.J., Kim, D.H., Moon, Y.S., Jung, J.S., Ahn, E.M., Baek, N.I., Song, D.K., 2004. Protection against beta-amyloid peptide-induced memory impairment with long-term administration of extract of Angelica gigas or decursinol in mice. Prog. Neuropsychopharmacol. Biol. Psychiatry 28, 25–30.
Yin, H., Guo, Q., Li, X., Tang, T., Li, C., Wang, H., Sun, Y., Feng, Q., Ma, C., Gao, C., Yi, F., Peng, J., 2018. Curcumin Suppresses IL-1beta Secretion and Prevents Inflammation through Inhibition of the NLRP3 Inflammasome. J. Immunol. 200, 2835–2846.
Zhang, H., Wang, Q., Sun, C., Zhu, Y., Yang, Q., Wei, Q., Chen, J., Deng, W., Adu-Frimpong, M., Yu, J., Xu, X., 2019. Enhanced oral bioavailability, anti-tumor activity and hepatoprotective effect of 6-shogaol loaded in a type of novel micelles of polyethylene glycol and linoleic acid conjugate. Pharmaceutics 11, 107.
Zhang, X., Tian, Y., Zhang, C., Tian, X., Ross, A.W., Moir, R.D., Sun, H., Tanzi, R.E., Moore, A., Ran, C., 2015. Near-infrared fluorescence molecular imaging of amyloid beta species and monitoring therapy in animal models of Alzheimer's disease. Proc. Natl. Acad. Sci. USA 112, 9734–9739.